Blue-Green Systems

Effective and selective removal of phosphate from water by the Co(II)-based adsorbent

Keke Han, Deng You, Penghui Shao, Liming Yang, Hui Shi*, Wanjun Yu, Shuiping Yu, Lili Fang, Xu Zhuang and Xubiao Luo

Key Laboratory of Jiangxi Province for Persistent Pollutants Control and Resources Recycle, Nanchang Hangkong University, Honggutan District, Fenghe South Street 696, Nanchang 330063, China

*Corresponding author. E-mail: shihui900501@126.com

Abstract

In this study, a novel Co(II)-based adsorbent Co-H_2L is developed for the removal of phosphate. The batch experiments demonstrate that the Co-H_2L possesses preferable ability of phosphate capture from water in mildly acidic to neutral pHs, with a maximum adsorption capacity of 194.44 mg P g^{-1}. Adsorption isotherms for phosphate agree with the Langmuir model, suggesting a monolayer process. The mechanism for phosphate adsorption onto Co-H_2L mainly followed the coordination mechanism, and the Co valence electron orbitals play the key role in the phosphate adsorption. In addition, the Co-H_2L adsorbent can selectively remove phosphate ions in the presence of the competing ions (Cl^-, NO_3^-, and SO_4^{2-}) at higher concentrations. Our results therefore indicate that the Co(II)-based adsorbent is expected to find extensive applications in phosphate removal for water management.

Key words: adsorption, Co(II)-based adsorbent, coordination, phosphate

INTRODUCTION

The excessive discharge of phosphorus-containing agricultural, industrial, and domestic wastewater has gained significant research interest in the past few years, mainly due to the harmful effects of eutrophication in aquatic environments (Kim et al. 2011). It is critical for the effective removal of excess phosphate from water to counteract eutrophication and restore water quality. Various methods including chemical precipitation, ion exchange, adsorption, and membrane process have been proposed for the phosphate removal (Luo et al. 2013; Kim et al. 2017; Yang et al. 2019). Among these technologies, the adsorption method becomes the most appealing one attributing to its advantages of simple operation, high efficiency, and environmental friendliness.

Recently, a variety of adsorbent systems have been proposed for phosphate ions removal, with transitional metal based adsorbents attracted much attention due to their excellent physical and chemical properties. Xie et al. and Fang et al. developed lanthanum hydroxide and its hybrids for the removal and recovery of phosphate from water (Xie et al. 2014a, 2014b; Fang et al. 2018). Harris and colleagues reported a catch-and-release system of gadolinium complexes for the selective removal of phosphate (Harris et al. 2017). However, these traditional adsorbents suffer from inherent limitations

of relatively low adsorption capacity or poor selectivity. Therefore, novel transitional metal based adsorbents with high capacity and good selectivity for phosphate removal are urgently necessary.

Cobalt (Co) compounds have also been employed for phosphate removal in water treatment. Hudson *et al.* reported that phosphate can be irreversibly adsorbed by $LiCoO_2$ material even at the environmentally relevant concentration of 1 micromolar (Hudson *et al.* 2000). Owing to the strong affinity between Co and PO_4 anions, the $Co_3 (PO_4)_2$ precipitate is inclined to be formed, therefore becoming the key to the chemistry behavior of Co and PO_4. As known, the La(III), Mg(II), and Fe(III)-based phosphate ions adsorbents are inclined to form precipitation of $LaPO_4$, $Mg_3(PO_4)_2$, and $FePO_4 \cdot 2H_2O$ (Chouyyok *et al.* 2010; Xie *et al.* 2014a, Pham *et al.* 2019) with solubility constant (K_{sp}) of 3.98×10^{-23}, 1.04×10^{-24}, and 9.91×10^{-16} (Meng 1988), respectively, while $Co_3(PO_4)_2$ shows comparatively lower K_{sp} of 2.05×10^{-35}. In this respect, Co(II)-based adsorbent exhibits great potential in high-efficiency and permanent sequestration of phosphate from water system.

Benzimidazole and its derivatives possessed various coordination modes and were liable to bond with metal ions to form oligomers or multi-dimensional frame structures, and metal organic complexes based on benzimidazole ligand have been successfully assembled. Liu *et al.* introduced the carboxymethyl into the two nitrogen atoms of the imidazole ring, obtaining the good coordination capacity (Liu *et al.* 2009). You *et al.* synthesized Cu(II)-1,3-dicarboxymethyl-2-methyl benzimidazole for the removal of antimonite and antiminate, both the experimental and theoretical studies illustrated the favorable adsorption capacity (You *et al.* 2017). However, to the best of our knowledge, there are no reports about cobalt-containing coordination complex as adsorbents to remove phosphate from water so far.

Therefore, the aim of the present study was to develop a novel metal coordination complex using Co(II) as the coordination ion and H_2L as the ligand for the effective and selective removal of phosphate. The effects of pH and co-existing ions on adsorption were investigated, and characterizations of SEM, EDS, EPR, FT-IR, and XPS were employed to evaluate structures and morphologies. Additionally, isotherm and kinetic studies were carried out to elucidate the mechanism and to determine the best fit of isotherm and kinetic models.

METHODS

Chemicals

Cobalt (II) chloride hexahydrate ($CoCl_2 \cdot 6H_2O$, 99%, Xilong Chemical Co., Ltd.), ethylene glycol dimethacrylate (EGDMA, 99%, J&K Chemical Ltd.), 2-methylbenzimidazole (98%, J&K Chemical Ltd.), potassium dihydrogen phosphate (KH_2PO_4, 99.5%, Xilong Chemical Co., Ltd.) were used directly as received. N,N'-dicarboxymethyl-2-methylbenzimidazole (H_2L) was synthesized as previously reported in the literature (You *et al.* 2017).

Synthesis of Co-H_2L adsorbents

Firstly, 2 mmol $CoCl_2 \cdot 6H_2O$ and 1 mmol H_2L were added to the mixed solvent of 15 mL ethanol and 15 mL deionized water, and ultrasonically mixed until completely dissolved. Then, 1 mL EGDMA was added into the reaction mixture with adjusted pH of 6, and ultrasonically mixed for 2 h to promote the coordination of the metal ion with the ligand. Finally, the resultant Co-H_2L adsorbent was separated by filtration and washed several times with water and ethanol, and then dried in an incubator at 60 °C for 24 h.

Batch adsorption experiments

The phosphate stock solution was prepared by dissolving accurately weighed KH_2PO_4 in deionized water. All batch adsorption experiments were performed with 20 mg Co-H_2L and 20 mL phosphate solutions at 30 °C in an incubator shaker (New Brunswick Scientific Co., Inc.) for 24 h to ensure the adsorption equilibrium.

The effect of pH on adsorption was evaluated under various initial pH values ranging from 3.0 to 12.0, which were adjusted with 0.1 M HCl or 0.1 M NaOH solution. Competitive adsorption experiments were performed by adding a certain amount of Na_2SO_4, NaCl, or $NaNO_3$ to investigate the effect of coexisting anions on phosphate adsorption. The initial concentration of phosphate was fixed at 1.0 mM, and the concentration of coexisting anions was 1.0 mM or 5.0 mM.

Isothermal adsorption experiments were carried out at 30 °C with different concentration of phosphate (15–600 mg P L^{-1}) at initial pH of 3.0. Adsorption kinetic experiments were performed by mixing 300 mg of Co-H_2L adsorbent with 300 mL phosphate solution with initial concentration of 530 mg P L^{-1} at pH of 4.8. At predetermined intervals, the samples were taken out from beakers and filtrated for the determination of phosphate concentration.

Cycle adsorption and regeneration experiments were taken to evaluate the reusability of Co-H_2L. The adsorbent dosage for the first cycle was 1 g L^{-1}, and the initial P concentration was 20 mg L^{-1}. The regeneration of the exhausted Co-H_2L was performed by using the 0.5 M $NaHCO_3$ solution stirring magnetically for 24 h at room temperature, washed with DI water and dried to obtain the regenerated material.

Characterizations and analytical methods

The morphology and elemental composition of Co-H_2L was examined using an SU 8020 scanning electron microscope (SEM, Hitachi, Japan) coupled with energy dispersive spectroscopy (EDS). The surface functionality was characterized by Fourier transform infrared (FT-IR) spectroscopy. Electron paramagnetic resonance (EPR) spectrum was recorded on a JES-FA200 EPR spectrometer. X-ray photoelectron spectroscopy (XPS) was probed with an ESCALAB-2 spectrometer. Zeta potentials were measured by a Zetasizer Nano ZS potential analyzer (Malvern Instruments Ltd., UK). The phosphate concentration was determined by the molybdenum blue spectrophotometric method through T6 UV-vis spectrometer (Pgeneral, China). The anions (SO_4^{2-}, Cl^-, and NO_3^-) concentrations were measured by ICS-1100 ion chromatography system (Dionex, China).

RESULTS AND DISCUSSION

Characterizations of Co-H_2L adsorbent

The surface morphology of Co-H_2L adsorbent was examined by SEM and displayed in Figure 1(a), the synthesized Co-H_2L was an amorphous inorganic complex with some tiny particles distributed on the surface. Meanwhile, the strong Co peaks were observed from the EDS spectrum (Figure 1(c)), suggesting that the Co atom has been combined with the H_2L ligand and the adsorbent has been successfully synthesized. The EPR spectrum of Co-H_2L exhibited a clear signal at g = 2.0509 (Figure 1(d)) corresponding to oxygen defects on the surfaces, which is beneficial for the phosphate adsorption (Xu et al. 2017).

As shown in Figure 1(b), phosphate adsorption on the Co-H_2L surface resulted in changes in morphology with the particles on the surface becoming more pronounced and the thickness of the material significantly increased. The FT-IR spectra of the adsorbent and phosphate loaded adsorbent
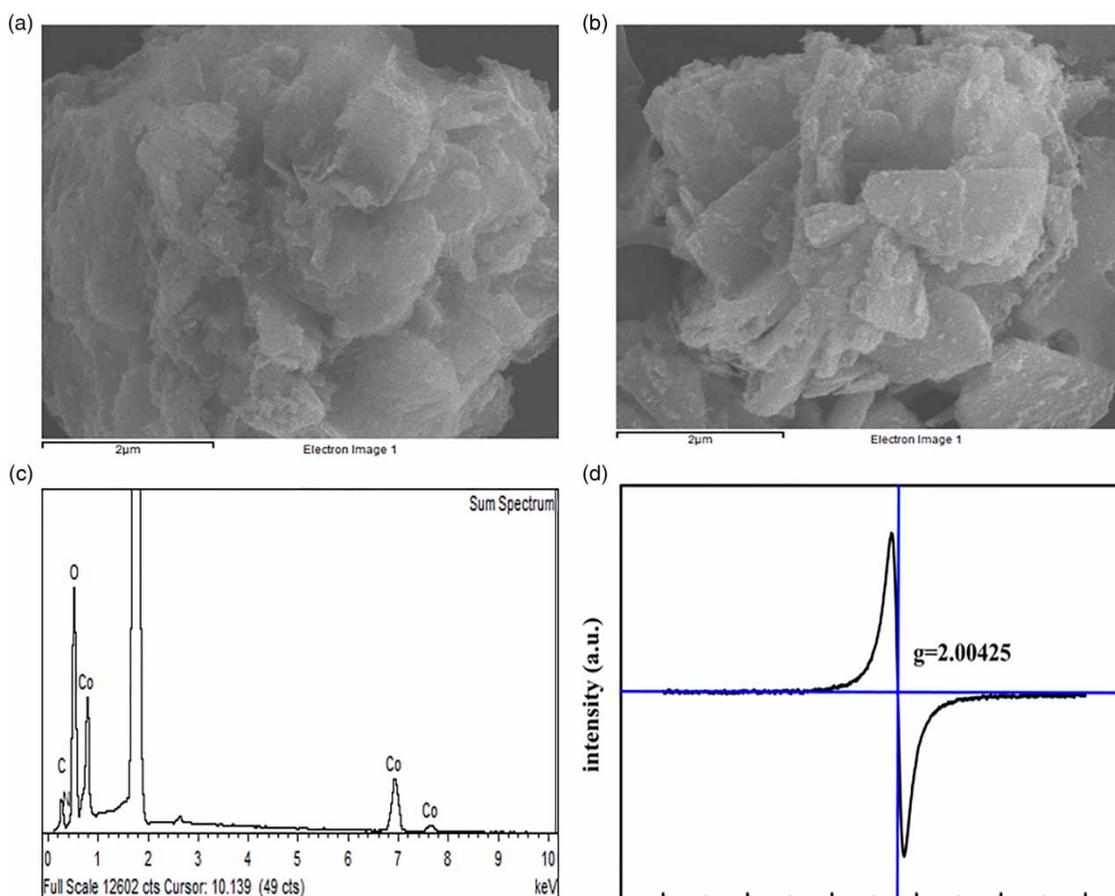
Figure 1 | SEM images of the adsorbent Co-H$_2$L (a) and Co-H$_2$L after the adsorption of 530 mg P L^{-1} phosphate (b). EDS spectrum of Co-H$_2$L (c). EPR spectrum of Co-H$_2$L at room temperature (d).

in the range of 500–3,500 cm^{-1} were provided in Figure 2. The FT-IR spectrum for Co-H$_2$L shows a strong peak at 1,628 cm^{-1}, which was assigned to the stretching vibration mode of ionized carboxyl group, and the small bands appeared at 1,475.43 cm^{-1}, 1,509.45 cm^{-1}, and 1,538.81 cm^{-1} belonged to the aromatic C $=$ C vibration. Typical P-O fingerprint features were identified in the frequency range of 900–1,200 cm^{-1} (Fang *et al.* 2017), where the two lower frequency features at 976 cm^{-1} and 937 cm^{-1} corresponded to the symmetric and asymmetric CoO-P vibrations (Laudadio *et al.* 2018). These results indicated that phosphate ions were adsorbed on Co-H$_2$L successfully.
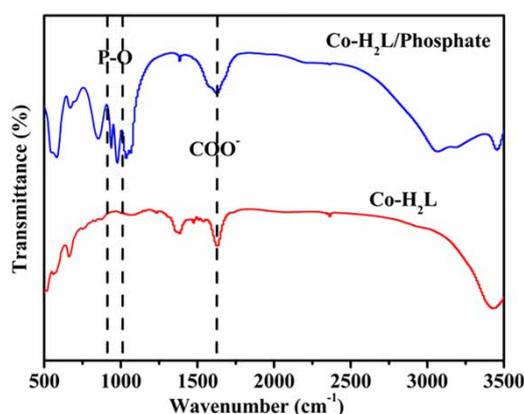

Figure 2 | FT-IR spectra of Co-H$_2$L before and after phosphate adsorption.

Adsorption performance

The surface charge plays an important role in the adsorption process, which determines the strength of electrostatic interaction between the adsorbate and the adsorbent. The relationship between zeta potentials of the Co-H_2L adsorbent and pH values of the solution was represented in Figure 3(a). The zeta potential followed a trend of decline over the whole pH range increasing from 3.0 to 12.0, with the isoelectric point around 7.0. It was found that the surface charge of Co-H_2L changed after phosphate adsorption, and the zeta potential decreased after adsorption at initial phosphate concentration of 530 mg P L^{-1}. Taking the pH conditions of 3.0 and 8.0 for example, the zeta potential decreased significantly from about $+35$ mV and -10 mV to $+20$ mV and -15 mV after phosphate adsorption, respectively.
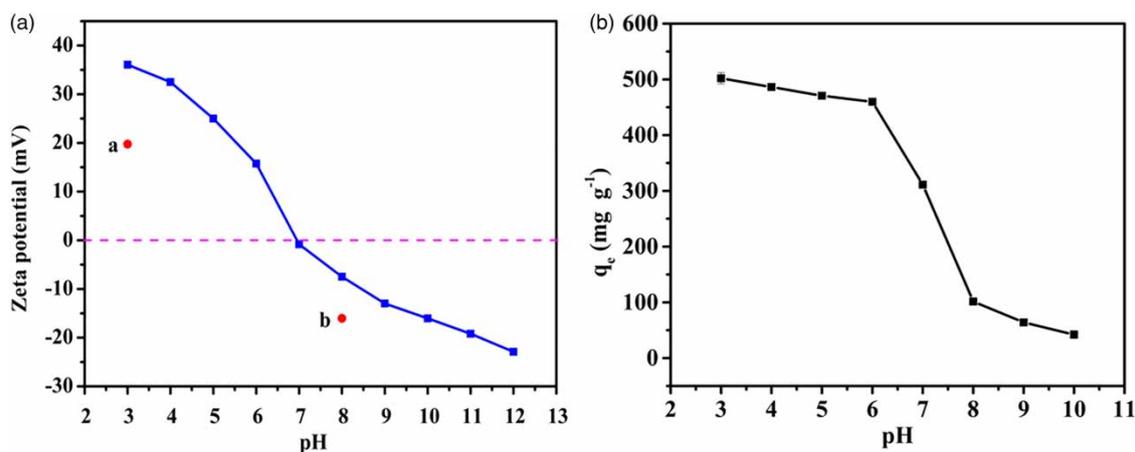

Figure 3 | (a) Zeta potential of Co-H_2L as the function of pH (solid line) and that of Co-H_2L with adsorbed PO_4 at pH = 3.0 (dot a) and pH = 8.0 (dot b). (b) The effect of pH on phosphate adsorption by Co-H_2L (C_0 = 330 mg P L^{-1}, adsorbent dosage = 1 g L^{-1}, reaction time = 24 h, T = 30 °C).

In addition to the impact on the surface charge of the adsorbent, pH also controls the adsorbate speciation in the solution, therefore significantly affecting adsorption capacities. Figure 3(b) illustrated the effect of pH on phosphate uptake onto Co-H_2L. It revealed a nearly constant phosphate adsorption capacity in the pH range of 3.0–6.0, with the highest adsorption capacity of 160 mg P g^{-1} at pH = 3.0. The result was possibly attributed to the electrostatic attraction between the Co-H_2L and phosphate ion at acidic pH, which not only achieved the immobilization of phosphate ions, but also provided favorable conditions for phosphate combination with metal sites on the surface of the adsorbent. By contrast, the adsorption capacity decreased dramatically at higher pH (>6.0), mainly due to the electrostatic repulsion between the deprotonated surface of Co-H_2L and highly charged phosphate anions (Figure 4).

Adsorption isotherms

The equilibrium relationship between the ion concentrations in the adsorbent/adsorbate interphases is illustrated by adsorption isotherms based on both the Langmuir (Equation (1)) and Freundlich (Equation (2)) linearized isotherm models:

$$Q_e = \frac{Q_m K_L C_e}{1 + K_L C_e} \tag{1}$$
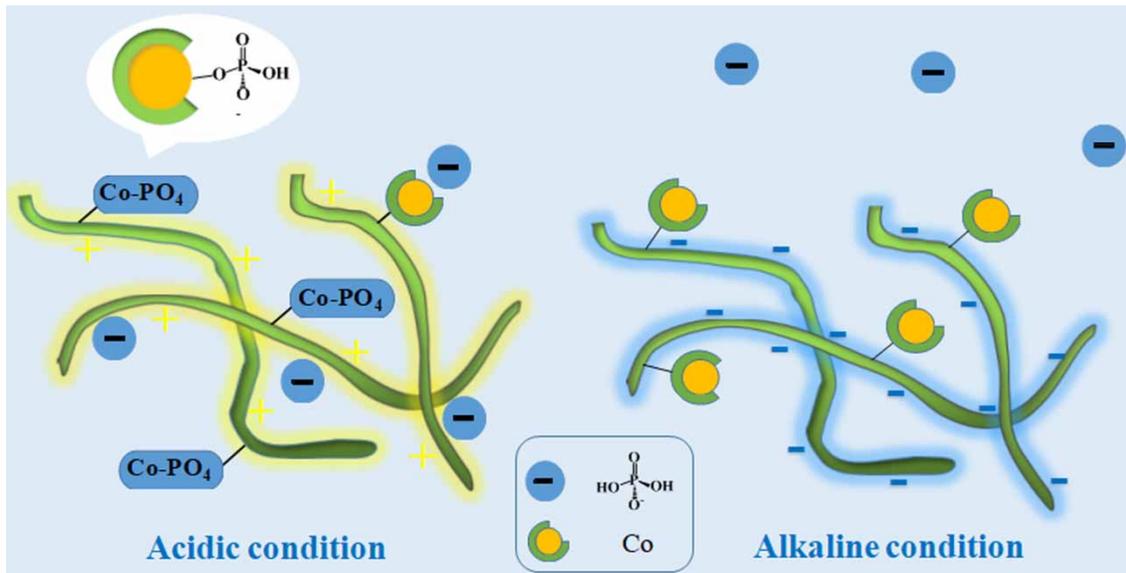
$$Q_e = K_F C_e^{\frac{1}{n}} \tag{2}$$

Figure 4 | Effects of pH on electrostatic force between the Co-H$_2$L and phosphate.

where C_e (mg L^{-1}) and Q_e (mg g^{-1}) are the equilibrium concentration and amount of phosphate adsorbed, respectively. As for the Langmuir model, Q_m (mg g^{-1}) is the maximum uptake capacity and K_L (L mg^{-1}) is the Langmuir constant. While for the Freundlich model, K_L (mg$^{1-(1/n)}$ L$^{1/n}$ g^{-1}) is the Freundlich constant that refers to the adsorption capacity and the strength of the adsorptive bond, and n is the heterogeneity factor represents the bond distribution, where $1 < n < 10$ suggests favorable adsorption (Shao *et al.* 2019).

Figure 5 displays the adsorption isotherm and the Langmuir and Freundlich model linear fitting to the experimental data. The corresponding fitting parameters are listed in Table S1. The n value in the Freundlich model was 4.11, showing strong affinity between the adsorbate and the adsorbent. The Langmuir and Freundlich model fitting correlation coefficients (R^2) for Co-H$_2$L were 0.98 and 0.70, respectively, which demonstrated that the phosphate adsorption process fit better with the Langmuir model than the Freundlich model, indicating that phosphate adsorption was a monolayer process. According to the Langmuir model fitting, the calculated theoretical maximum adsorption capacity of Co-H$_2$L was 194.44 mg P g^{-1}. Additionally, the maximum adsorption capacity of the Co-H$_2$L for phosphate anions was compared with other representative adsorbents reported in the literature. As summarized in Table 1, the Co-H$_2$L exhibited a significantly higher adsorption capacity than all other adsorbents ever reported, suggesting that the Co-H$_2$L adsorbent could be a promising candidate for the phosphate removal from wastewater.
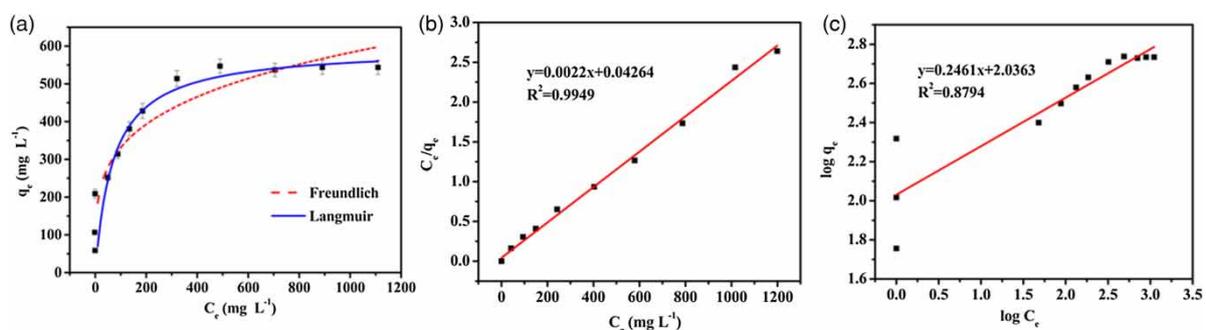

Figure 5 | (a) The adsorption isotherm of Freundlich and Langmuir for phosphate onto Co-H$_2$L at pH = 3.0. The dashed and solid line is the corresponding fitting curve based on the Freundlich and Langmuir equations, respectively (adsorbent dosage = 1 g L^{-1}, reaction time = 24 h, T = 30 °C). (b) Langmuir model linear fitting. (c) Freundlich model linear fitting.

Table 1 | Adsorption performance of the Co-H$_2$L and other representative adsorbents reported in the literature

Adsorbents	pH	Adsorption capacity (mg P g^{-1})	References
Fe-EDA-SAMMS	5	14.25	Chouyyok *et al.* (2010)
Fe-Mn binary oxide	5.6	36	Zhang *et al.* (2009)
Graphene-La$_2$O$_3$	6.2	82.6	Chen *et al.* (2016)
Mg(OH)$_2$	NA	52.08	Xie *et al.* (2014a)
HZO	6	31.9	Qiu *et al.* (2015)
LAH-10	4	128.2	Xu *et al.* (2017)
La-ZB	6	106.2	Pham *et al.* (2019)
L-Y(OH)$_3$	5	90.8	Kim *et al.* (2017)
Co-H$_2$L	3	194.44	This work

Adsorption kinetics

Kinetic parameters are required for the design of large-scale adsorption processes and the indication of adsorbent performance. Kinetic behavior of phosphate uptake by Co-H$_2$L was investigated at room temperature, and the pseudo-first order (Equation (3)) and pseudo-second order kinetic models (Equation (4)) listed below were employed to describe the adsorption kinetics.

$$Q_t = Q_e - Q_e e^{-K_1 t} \tag{3}$$

$$Q_t = \frac{K_2 Q_e^2 t}{1 + K_2 Q_e t} \tag{4}$$

where Q_t and Q_e are the amount of phosphate adsorbed on the Co-H$_2$L adsorbent surface (mg g^{-1}) at t min and at equilibrium, respectively. k_1 and k_2 are the rate constants of the pseudo-first order and pseudo-second order models, respectively. Generally, the pseudo-first order model fits better in the initial stage of reaction processes especially those with rapid adsorption, while the pseudo-second order model considers adsorption behavior over longer contact times with chemisorption as the rate controlling process (Crini *et al.* 2007).

Figure 6(a) shows the adsorption behavior of Co-H$_2$L as a function of reaction time in 530 mg P L^{-1} aqueous phosphate solutions. The kinetic curves show a fast initial phosphate uptake followed by a slower process to reach complete equilibrium after 2 h. The obtained kinetic parameters are summarized in Table S2, and the corresponding fitting curves are displayed in Figure 6(b) and 6(c). The correlation coefficients of the pseudo-first order and pseudo-second order kinetics are determined
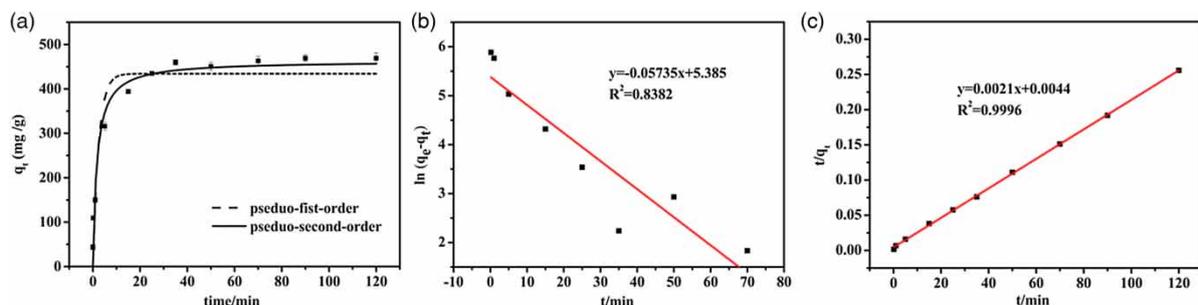

Figure 6 | (a) Adsorption kinetics of phosphate onto Co-H$_2$L at room temperature. The dashed and solid lines are the corresponding fitting curve based on the pseudo-first-order and pseudo-second-order equation, respectively (adsorbent dosage = 1 g L^{-1}, C$_0$=530 mg P L^{-1}). (b) Pseudo-first-order kinetic plots. (c) Pseudo-second-order kinetic plots.

to be 0.923 and 0.953, and the theoretical Q_e values derived from the pseudo-first order and pseudo-second order model are 141.7 and 151.04 mg P g^{-1}, respectively. It is illustrated that the adsorption of phosphate followed the pseudo-second order kinetic model with the good linearity and the well-matched experimental and calculated Q_e values, indicating that the chemisorption is primarily responsible for the phosphate adsorption onto Co-H$_2$L and thus indicative of strong bonding between phosphate and the Co-H$_2$L adsorbent.

Adsorption mechanism

In order to explain the mechanism for the phosphate adsorption, XPS were applied to investigate the changes of Co-H$_2$L before and after adsorption and uncover the detailed adsorption sites of Co-H$_2$L. As displayed in Figure 7(d), the O 1 s spectra were split into three overlapped peaks at the binding energy of 530.71, 531.11, and 532.51 eV, corresponding to the Co-O, C = O, and C-O in the Co-H$_2$L adsorbent, respectively (Zhou *et al.* 2016; Laudadio *et al.* 2018). The peak at 529.41 eV originating from P-O appeared after phosphate adsorption (Fang *et al.* 2015) (Figure 7(a)), which was consistent with the results of the FT-IR. It was worth noting that the peak intensity of Co-O also changed after phosphate adsorption, which could be explained by assuming that the vacant orbital of the Co atom was coordinated with the lone-pairs of the O atom of the phosphate molecule. In order to further demonstrate that the vacant orbital of the Co atom attained coordination, the peaks at a binding energy of 781.02 eV and 2.25 eV were assigned to Co 2p and Co valence electron orbitals (d^{2}sp^1 hybrid orbital). As shown in Figure 7(b) and 7(e), there were no significant changes for the peaks of Co 2p after phosphate adsorption, while the peaks of Co valence electron orbitals shifted from 2.25 eV to 2.85 eV during the adsorption process (Figure 7(c) and 7(f)). These results verified the coordination mechanism and the indispensable role of Co valence electron orbitals for the phosphate adsorption.
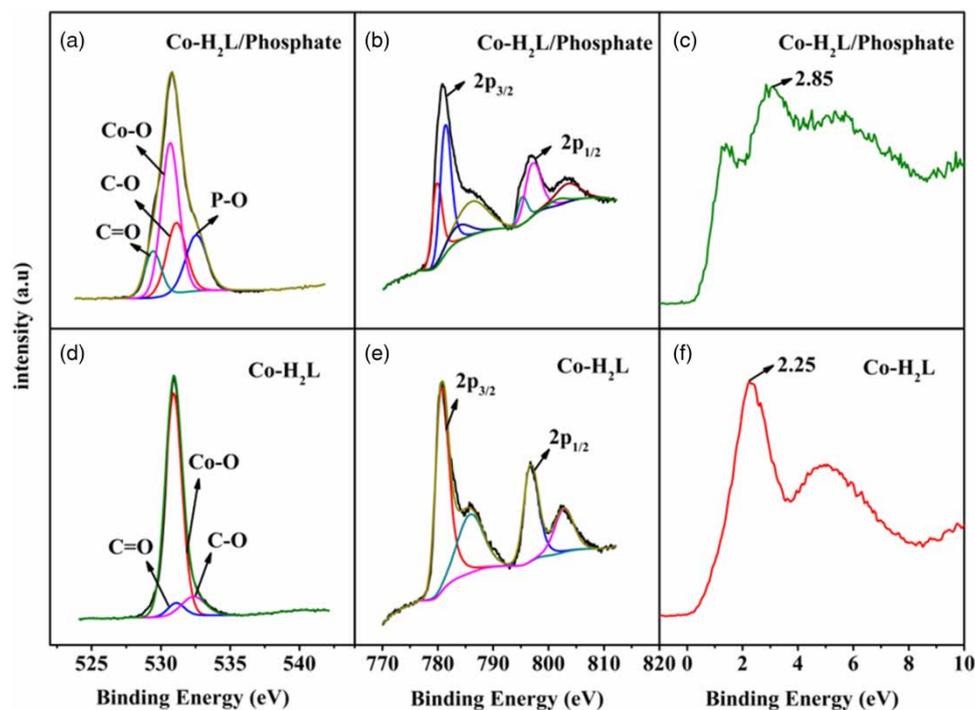

Figure 7 | XPS characteristics of Co-H$_2$L before and after phosphate adsorption. O 1 s (a), Co 2p (b), and Co valence electron orbitals (c) energy after adsorption; O 1 s (d), Co 2p (e), and Co valence electron orbitals (f) energy before adsorption.

Effect of co-existing anions on phosphate adsorption

It is established that the wastewater usually contains co-existing anions along with phosphate. Considering the possible interference of the co-existing anions, the selectivity of Co-H$_2$L toward phosphate was evaluated by adding some typical anionic species including SO$_4^{2-}$, Cl$^-$, and NO$_3^-$ into the reaction mixtures, as shown in Figure 8. As for the Cl$^-$ and NO$_3^-$, the adsorption effect of Co-H$_2$L was negligible, while the SO$_4^{2-}$ showed relatively higher adsorption capacity and it increased with the increase of the SO$_4^{2-}$ concentration, which might be ascribed to the easier adsorption of multivalent anions than monovalent anions. It was worth noting that the presence of the competing anions of SO$_4^{2-}$, Cl$^-$, and NO$_3^-$ exhibited no significant influence on the adsorption capacity of phosphate even for their concentrations of 5 times higher than phosphate, revealing satisfactory anti-interference ability of the Co-H$_2$L adsorbent. It was speculated that the solubility of different cobalt salts determined the high selectivity, the cobalt chloride, cobalt sulfate, and cobalt nitrate are soluble salts, while cobalt phosphate is highly susceptible to form precipitation. In this respect, Co-H$_2$L adsorbent is more likely to bind to phosphate. The favorable performance of the Co-H$_2$L on the tolerance of foreign species is crucial for the practical applications.
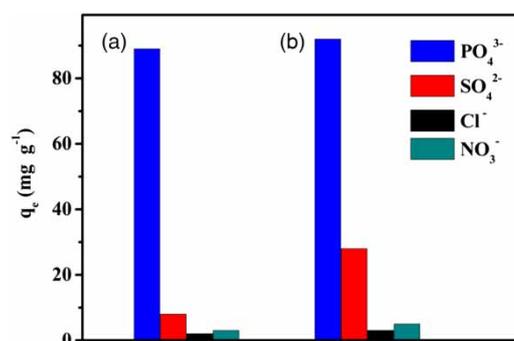

Figure 8 | Interference effects of common anions on the phosphate adsorption on Co-H$_2$L adsorbent. The residual phosphate concentrations in filtrates were measured after adsorption in 1 mM (95 mg PO$_4$ L^{-1}) KH$_2$PO$_4$ solutions containing competing anions (SO$_4^{2-}$, Cl$^-$, and NO$_3^-$) of (a) 1 mM and (b) 5 mM for 24 h.

Recyclability of Co-H$_2$L

Cycle adsorption and regeneration of batch experiments were taken to evaluate the reusability of Co-H$_2$L for phosphate removal. Figure 9 illustrated the variation in adsorption and desorption efficiency during the recycle processes. Although the capacity of phosphate adsorption was somewhat decreased with increasing adsorption/desorption processes, five times regenerated adsorbent still exhibited over 70% adsorption efficiency, and the desorption efficiency also maintained approaching 90% even after five sorption-regeneration cycles, indicating the potential of the proposed Co-H$_2$L materials in phosphate sequestering as a sustainable adsorbent.

CONCLUSIONS

In summary, we have introduced a novel metal coordination complex of Co-H$_2$L for the removal of phosphate in the water system. As a result, the phosphate removal by Co-H$_2$L was most successful from acidic to neutral pH range, and a state-of-the-art adsorption capacity of 194.44 mg P g^{-1} was achieved. Adsorption isotherms for phosphate fitted in to the Langmuir model and were thus indicative of a monolayer process, and the adsorption kinetics followed the pseudo-second order model,
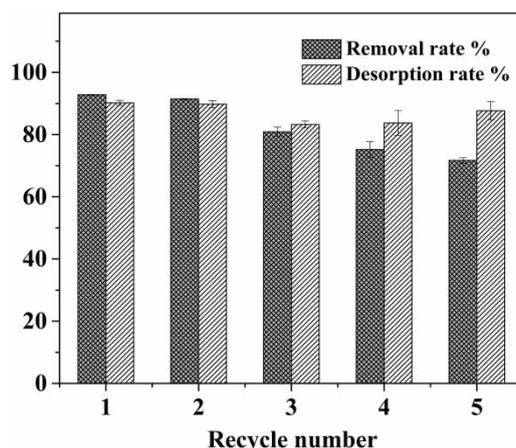
Figure 9 | Cycle adsorption and desorption of batch experiments for Co-H$_2$L (initial $P = 20$ mg P L^{-1}; adsorption dose $= 1$ g L^{-1}; T $= 303.15$ K).

suggesting that the adsorption mainly occurs through chemisorption. The XPS study confirmed the coordination mechanism and the integral role of Co valence electron orbitals for the phosphate adsorption. Moreover, the negligible effect of the co-existing ions indicated the good selectivity of the synthesized adsorbent. The novel adsorbent with competitive adsorption capacity and good selectivity can be a promising candidate for the phosphate removal from water.

ACKNOWLEDGEMENTS

REFERENCES

Chen, M. L., Huo, C. B., Li, Y. K. & Wang, J. H. 2016 Selective adsorption and efficient removal of phosphate from aqueous medium with graphene-lanthanum composite. *ACS Sustainable Chemistry and Engineering* **4** (3), 1296–1302.

Chouyyok, W., Wiacek, R. J., Pattamakomsan, K., Sangvanich, T., Grudzien, R. M., Fryxell, G. E. & Yantasee, W. 2010 Phosphate removal by anion binding on functionalized nanoporous sorbents. *Environmental Science and Technology* **44** (8), 3073–3078.

Crini, G., Peindy, H. N., Gimbert, F. & Robert, C. 2007 Removal of C.I. basic green 4 (malachite green) from aqueous solutions by adsorption using cyclodextrinbased adsorbent: kinetic and equilibrium studies. *Separation and Purification Technology* **53** (1), 97–110.

Fang, L. P., Huang, L. Z., Holm, P. E., Yang, X. F., Hansen, H. C. B. & Wang, D. S. 2015 Facile upscale synthesis of layered iron oxide nanosheets and its application for phosphate removal. *Journal of Materials Chemistry A* **3** (14), 7505–7512.

Fang, L. P., Shi, Q. T., Nguyen, J., Wu, B., Wang, Z. M. & Irene, M. C. L. 2017 Removal mechanisms of phosphate by lanthanum hydroxide nanorods: investigations using EXAFS, ATRFTIR, DFT and surface complexation modeling approaches. *Environmental Science and Technology* **51** (21), 12377–12384.

Fang, L. P., Liu, R., Li, J., Xu, C. H., Huang, L. Z. & Wang, D. S. 2018 Magnetite/Lanthanum hydroxide for phosphate sequestration and recovery from lake and the attenuation effects of sediment particles. *Water Research* **130**, 243–254.

Harris, S. M., Nguyen, J. T., Pailloux, S. L., Mansergh, J. P., Dresel, M. J., Swanholm, T. B., Gao, T. & Pierre, V. C. 2017 Gadolinium complex for the catch and release of phosphate from water. *Environmental Science and Technology* **51** (8), 4549–4558.

Hudson, J. J., Taylor, W. D. & Schindler, D. W. 2000 Phosphate concentrations in lakes. *Nature* **406**, 54–56.

Kim, J., Li, W., Philipsc, B. & Grey, C. 2011 Phosphate adsorption on the iron oxyhydroxides goethite (a-FeOOH), akaganeite (b-FeOOH), and lepidocrocite (g-FeOOH): a 31P NMR study. *Energy and Environmental Science* **4** (10), 4298–4305.

Kim, M., Kim, H. & Byeon, S. 2017 Layered yttrium hydroxide l-$Y(OH)_3$ luminescent adsorbent for detection and recovery of phosphate from water over a wide pH range. *ACS Applied Materials and Interfaces* **9** (46), 40461–40470.

Laudadio, E. D., Bennett, J. W., Green, C. M., Mason, S. E. & Hamers, R. J. 2018 Impact of phosphate adsorption on complex cobalt oxide nanoparticle dispersibility in aqueous media. *Environmental Science and Technology* **52** (17), 10186–10195.

Liu, Z. L., Wang, B., Li, G., Wang, L., Meng, X. & He, Z. 2009 Polymeric frameworks constructed from bulky carboxylates and 4,4-bipyridine linkages: synthesis, crystal structures, and properties. *Crystal Growth and Design* **9** (12), 5244–5258.

Luo, X. B., Wang, C. C., Wang, L. C., Deng, F., Luo, S. L., Tu, X. M. & Au, C. 2013 Nanocomposites of graphene oxide-hydrated zirconium oxide for simultaneous removal of As(III) and As(V) from water. *Chemical Engineering Journal* **220**, 98–106.

Meng, Q. Z. 1988 *Inorganic Chemistry*. Beijing Normal University Press, Beijing.

Pham, T., Lee, K., Kim, M. S., Seo, J. & Lee, C. 2019 La-modified ZSM-5 zeolite beads for enhancement in removal and recovery of phosphate. *Microporous and Mesoporous Materials* **279**, 37–44.

Qiu, H., Liang, C., Zhang, X. L., Chen, M. D., Zhao, Y. X., Tao, T., Xu, Z. W. & Liu, G. 2015 Fabrication of a biomass-based hydrous zirconium oxide nanocomposite for preferable phosphate removal and recovery. *ACS Applied Materials and Interfaces* **7** (37), 20835–20844.

Shao, P., Ding, L., Luo, J., Luo, Y., You, D., Zhang, Q. & Luo, X. 2019 Lattice defect-enhanced adsorption of arsenic on zirconia nanospheres: a combined experimental and theoretical study. *ACS Applied Materials and Interfaces* **11** (33), 29736–29745.

Xie, F. Z., Wu, F. C., Liu, G. J., Mu, Y. S., Feng, C. L., Wang, H. H. & Giesy, J. P. 2014a Removal of phosphate from eutrophic lakes through adsorption by in situ formation of magnesiumhydroxide from diatomite. *Environmental Science and Technology* **48** (1), 582–590.

Xie, J., Wang, Z., Lu, S. Y., Wu, D. Y., Zhang, Z. J. & Kong, H. N. 2014b Removal and recovery of phosphate from water by lanthanum hydroxide materials. *Chemical Engineering Journal* **254**, 163–170.

Xu, R., Zhang, M. Y., Mortimer, R. J. G. & Pan, G. 2017 Enhanced phosphorus locking by novel lanthanum/aluminum-hydroxide composite: implications for eutrophication control. *Environmental Science and Technology* **51** (6), 3418–3425.

Yang, L., Yi, G., Hou, Y., Cheng, H., Luo, X., Pavlostathis, S. G., Luo, S. & Wang, A. 2019 Building electrode with three-dimensional macroporous interface from biocompatible polypyrrole and conductive graphene nanosheets to achieve highly efficient microbial electrocatalysis. *Biosensors & Bioelectronics* **141**, 111444.

You, D., Min, X. Y., Liu, L. L., Ren, Z., Xiao, X., Pavlostathis, S. G., Luo, J. M. & Luo, X. B. 2017 New insight on the adsorption capacity of metallogels for antimonite and antimonate removal: from experimental to theoretical study. *Journal of Hazardous Materials* **346**, 218–225.

Zhang, G., Liu, H., Liu, R. & Qu, J. 2009 Removal of phosphate from water by a Fe-Mn binary oxide adsorbent. *Journal of Colloid and Interface Science* **335** (2), 168–174.

Zhou, Y., Dong, C. K., Han, L. L., Yang, J. & Du, X. W. 2016 Top-down preparation of active cobalt oxide catalyst. *ACS Catalysis* **6** (10), 6699–6703.